

Received 24 May 2022, accepted 10 June 2022, date of publication 15 June 2022, date of current version 28 June 2022.

Digital Object Identifier 10.1109/ACCESS.2022.3183348

Joint Vector Sensor Beam Steering and Passive Time Reversal for Underwater Acoustic Communications

FABRICIO A. BOZZI¹ AND SÉRGIO M. JESUS¹, (Member, IEEE)

Laboratory for Robotics and Engineering Systems, University of Algarve, 8005-135 Faro, Portugal

Corresponding author: Fabricio A. Bozzi (fabozzi@ualg.pt)

This work was supported in part by the Brazilian Navy Postgraduate Study Abroad Program, Grant Port 227/MB/2019.

ABSTRACT This paper investigates how to advantageously combine acoustic vector sensor field components for underwater communications. The joint vector sensor beam steering and passive time-reversal receiver structure is proposed and compared against beam steering and standard passive time-reversal separately. The beam steering method takes into account proper directions in order to benefit from highly correlated channels. On the other hand, passive time-reversal was weighted to avoid combinations of possible noisy channels. Performance of receiver structures are quantified using simulation and recorded data from a shallow-water field experiment. In this experiment, a four-element three-dimensional vector sensor array was tied to a drifting ship receiving coherent communication signals from a bottom-moored sound source. Analytical expressions and a numerical simulation based on the experimental acoustic scenario indicate a relationship between source-receiver ranges and the vector sensor channels correlation, providing an initial understanding of the suitability of each receiver structure. Then, using individual or combined vector sensors, such structures were tested with experimental data, where the range relationship hypothesis from the simulation was nearly confirmed. Error analysis shows that shorter ranges favor the beam steering, whereas channel diversity is mostly explored in longer ranges. Furthermore, the proposed joint method, designed for vector sensors, has achieved up to ten times less error than individual approaches, also showing the benefit of exploring beamforming and diversity together.

INDEX TERMS Underwater acoustic communications, acoustic vector sensor, directional sensors, underwater acoustics array signal processing.

I. INTRODUCTION

Acoustic vector sensors are devices that separately measure acoustic pressure and directional components of the acoustic field [1]. Properly combining those measures allows to estimate sound wave direction using a single vector sensor. Over the last 20 years, vector sensors have been used in several applications, such as source localization [2], passive acoustic monitoring [3], sea bottom characterization [4], and underwater acoustic communications (UWAC) [5].

Within vector sensors, an omnidirectional hydrophone is used for sensing the acoustic pressure, whereas the directional components are usually related to the acoustic particle velocity measurement [5]–[7]. Particle velocity can be either

directly obtained by velocity-sensitive sensors (or derivatives), commonly based on inertial sensors, or estimated by pressure-gradient sensors, where pairs of hydrophones are used. Vector sensors that use inertial sensors, referred to as accelerometer-based vector sensors, are said to provide a true measurement of particle velocity. The advantages of accelerometer-based vector sensors are the wide dynamic range and bandwidth, although its high sensitivity to movement may be a drawback [7]–[9]. Pressure-gradient vector sensors provide particle velocity estimation, where the finite difference operation limits the dynamic range, and the pair of hydrophones needs to be accurately calibrated and matched. Moreover, as pressure-gradient models sense pressure, they are not so affected by non-acoustic interference, such as turbulence and flow noise, as those based on accelerometers [7]. Even if other vector sensor technologies exist

The associate editor coordinating the review of this manuscript and approving it for publication was Chengpeng Hao¹.

(e.g., see [9], [10] and references therein), the principle is that by sensing pressure and particle velocity, the acoustic field can be represented as a vector. Moreover, a shared claimed advantage of vector sensors regards their compactness compared to pressure-only arrays.

Hydrophone arrays, referred to here as pressure-only arrays, have been used for UWAC providing spatial processing gain. Studies show that the performance of diversity and beamforming methods are dependent on spatial and temporal signal coherence and the array configuration (i.e., number of sensors, length, and spacing) [11], [12]. Reducing the array aperture for a fixed wavelength and the same number of sensors favors beamforming since signal spatial coherence increases. Otherwise, expanding the aperture leads to uncorrelated signals, where diversity methods are advantageous.

Vector sensor signal correlation, considering UWAC multipath issues, was firstly addressed in 2009 [13]. That theoretical study provides correlation expressions for a single vector sensor or between two vector sensors. Analytical expressions took into account vector sensor spacing, frequency, and angle-of-arrival (AoA) spreading. Important insights, under Gaussian distribution assumption and small AoA spreading, show that pressure and particle velocity components can be totally uncorrelated. What makes sense for spherically isotropic noise, presented in [14], may also be applied for symmetric AoA signals in vector sensor components. Moreover, even if not so emphasized in that work, an interesting relationship is that vector sensor components may also be totally correlated, which generalizes the results for an intensity sensor, mostly considered in direction of arrival (DoA) studies. In this regard, the understanding of methods that explore both scenarios may lead to an improvement in performance. Even though, in practice, we may face a situation of partial correlation.

Although analytical expressions help to understand the characteristics of particle velocity components, practical receiver structures for UWAC were not addressed in [13], and a receiver for single input multiple output (SIMO) system was then proposed [15]. That receiver, based on passive time-reversal (PTR), is tested with experimental data. Results of communication performance have shown that for short (<300 m) and medium (>800 m) ranges, a single vector sensor outperforms a 40 cm pressure-only array. However, since that employed PTR structure is nonexclusive for vector sensors, e.g., it was also used with a pressure-only array in that work, we may think if a specific design for vector sensors, taking advantage of the directional information, could enhance such performance. For instance, applying variable gains for the horizontal directional components in order to emphasize components in the source direction. Furthermore, the benefit of such standard PTR structure was not evident when channels were highly correlated, and thus, a beamforming approach may be preferable. Studies that use standard beamforming approaches have shown the expected communication performance gain due to the SNR improvement [16], [17]. However, those works are limited to horizontal vector

sensors, and the details of the experiments, receiver structures, and data analysis are reduced.

Thus, this paper compares the communication performance of receiver structures for vector sensors. To the best of our knowledge, this is the first paper that uses a three-dimensional vector sensor joining beam steering and passive time-reversal. The use of an accelerometer-based 3D vector sensor in a challenging communication experiment is not commonly described in the literature, and it is a rare opportunity to validate such a proposed structure. This structure aims to explore extreme channel correlation scenarios taking advantage of both diversity and beamforming gain, even for a single vector sensor. Moreover, to demonstrate the proposed joint method benefit, it is compared against separated beam steering and standard PTR receivers. Results from simulation suggest that beamforming is better suited for shorter ranges, whereas diversity is for longer ranges. This evidence was nearly confirmed with real data, where the joint method has shown robustness along with the tested ranges.

This paper is organized as follows: data model equations for vector sensors are shown in Section II; vector sensor channel correlation analysis is shown in Section III; the receiver structure is presented in Section IV; Section V presents and discusses the results for simulation and experimental data; and finally, Section VI presents the conclusion.

II. DATA MODEL

The general system equation for a single vector sensor with n components can be defined as:

$$r_n = h_n \otimes s + w_n, \quad (1)$$

where r_n are the received pressure/particle velocity signals, h_n are the pressure/particle velocity channel impulse response (CIR), s is the transmitted signal, and w_n is the spherically-isotropic noise. The subscript n , from 1 to 4, refers to the pressure component ($\llbracket p \rrbracket$) and to the particle velocity components ($\llbracket v_x \rrbracket$, $\llbracket v_y \rrbracket$, $\llbracket v_z \rrbracket$), respectively. The symbol \otimes stands for time convolution, and for the particle velocity components, the adopted index convention are x and y to horizontal directions and z to the vertical.

The relation between pressure and particle velocity can be defined by the fundamental Euler's equation, taking v in evidence:

$$v = -\frac{1}{j\omega\rho_0} \nabla p, \quad (2)$$

where ∇ is the gradient operator, p is the pressure, ρ_0 is the medium static density, $j = \sqrt{-1}$, and v is the particle velocity. Equation (2) shows that pressure-gradient is proportional to particle velocity, and under the plane-waves condition, this latter can be converted to the same unity as pressure using:

$$p_v = -\rho_0 c v, \quad (3)$$

where the product $\rho_0 c$ is the acoustic impedance and p_v is the so-called, pressure-equivalent particle velocity. Replacing (3)

in (2) using Cartesian coordinates gives:

$$p_{vx} = \frac{1}{jk} \frac{\partial p}{\partial x}, \quad p_{vy} = \frac{1}{jk} \frac{\partial p}{\partial y}, \quad p_{vz} = \frac{1}{jk} \frac{\partial p}{\partial z}, \quad (4)$$

where k is the wave vector. Thus, particle velocity components can be analyzed as pressure-equivalent particle velocity components. Readers may notice that particle velocity will also refer to pressure-equivalent particle velocity hereafter.

III. PRESSURE AND PARTICLE VELOCITY CORRELATION

Correlation analysis of pressure and particle velocity components is crucial to understand the essence of the receiver structures to be presented in the next section. The present work does not intend to model the pressure or particle velocity acoustic channels. However, it can use existent correlation expressions developed in [13] to analyze two hypothetical scenarios for shallow water. First, when the source-receiver range is much larger than the water column (far-field) and horizontal propagation is predominant. Second, when the source-receiver range is short and vertically separated (source and receiver at different depths), which means source-receiver propagation is not predominantly horizontal.

Consider a single collocated vector sensor with pressure (p), horizontal (y), and vertical (z) components receiving B bottom and S surface arrivals. Assuming a small AoA spread, a Gaussian probability density function (PDF) is adopted with mean elevation angle μ and variance σ . Under these assumptions, channel cross-correlation may be given as follows [13]:

$$\begin{aligned} C^{py} &= \Lambda \cos \mu_b + (1 - \Lambda) \cos \mu_s, \\ C^{pz} &= \Lambda \sin \mu_b + (1 - \Lambda) \sin \mu_s, \\ C^{zy} &= \Lambda(1 - \sigma_b^2) \sin \mu_b \cos \mu_b \\ &\quad + (1 - \Lambda)(1 - \sigma_s^2) \sin \mu_s \cos \mu_s, \end{aligned} \quad (5)$$

where, bottom arrivals have mean elevation angles μ_b (positive by definition) and AoA spread σ_b , while surface arrivals have mean μ_s (negative by definition) and AoA spread σ_s . Moreover, Λ is the normalized amount of power scattering that comes from B bottom arrivals and $1 - \Lambda$ is the power scattering that comes from S surface arrivals. Equation (5) shows that pressure and particle velocity components present a sine/cosine pattern, whereas particle velocity channel cross-correlation presents a sine/cosine product pattern, which is weighted by the angle spread.

Expressions shown in (5) can be visualized in Fig. 1 for varying bottom and surface arrival angles. Differently of the analysis shown in [13], where the focus was on the correlation between spaced vector sensor components, here, a single collocated vector sensor is analyzed. Fig. 1 (a) represents a far-field scenario and shows that pressure and horizontal particle velocity correlation (C^{py}) are highly correlated (> 0.8) for predominant horizontal arrivals, which can be represented by angles not steeper than 20° as shown by red boxes. In this figure, C^{py} would be lower than 0.5 for steeper arrivals from 45° to 90° , which can represent late arrivals. For C^{pz} , a low

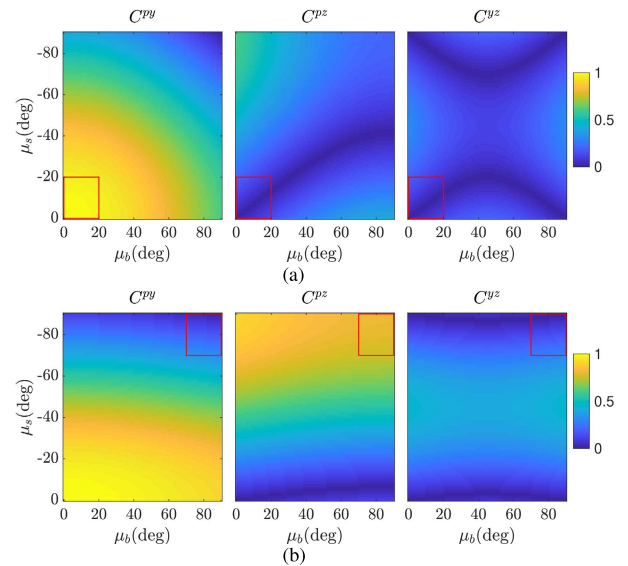


FIGURE 1. Pressure and particle velocity channel cross-correlations for varying bottom/surface mean value arrivals (μ_b and μ_s), using (5). Bottom and surface arrival spreads (σ_b and σ_s) are 10° and 1° , respectively. Far-field scenario with bottom power scattering $\Lambda = 0.4$ (a), and close-range scenario with $\Lambda = 0.1$ (b).

level of correlation is verified, which can be explained due to the sine symmetry, $\sin(-\mu) = -\sin(\mu)$, resulting in C^{pz} nearly zero for symmetric arrivals (it is not zero since $\Lambda = 0.4$). At last, particle velocity components cross-correlation present small values. This can be explained by the orthogonality between vertical and horizontal channels. Thus, analysis of Fig. 1 (a) suggests that pressure and the horizontal components are suitable for methods that explore channel coherence. Otherwise, pressure and the vertical component favor diversity methods, since their correlation is low.

The correlation analysis for close-range scenarios can be made by analyzing Fig. 1 (b). In this case, μ_b and μ_s are steeper (close to $\pm 90^\circ$, as shown in red boxes). The correlation between pressure and horizontal particle velocity is low (< 0.5), as C^{py} is cosine dependent. The opposite is verified for pressure and vertical particle velocity correlation, which is highly correlated (> 0.8) as it is sine-dependent and Λ presents low values. On the other side, horizontal and vertical particle velocity correlation present small values due to orthogonality.

Thus, these two extreme scenarios show that correlations among vector sensor components are variable, and receiver structures may explore vector sensor outputs according to a high/low cross-correlation assumption.

IV. JOINT VECTOR SENSOR BEAM STEERING AND PASSIVE TIME-REVERSAL

Fig. 2 shows the proposed joint vector sensor beam steering and passive time-reversal receiver structure (vs-bsptr) composed of noise normalization, Doppler compensation, joint beam steering and passive time-reversal, and a multichannel

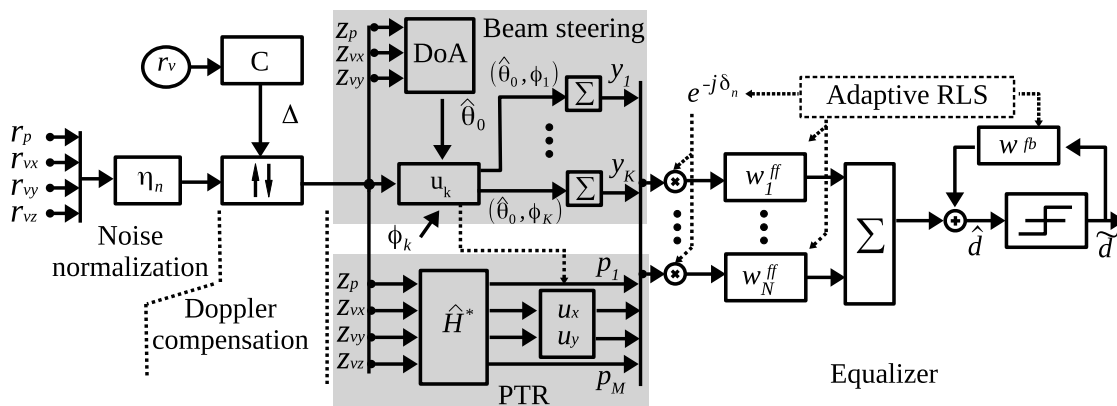


FIGURE 2. Joint vector sensor beam steering and passive time-reversal receiver structure for a single vector sensor. Input signals are pressure (r_p) and pressure-equivalent particle velocities (r_{vx}, r_{vy}, r_{vz}). In the beam steering segment, pressure and horizontal particle velocity components are used to estimate azimuth angle $\hat{\theta}_0$. Three elevation angles are chosen ($\phi_k = -90^\circ, 0^\circ, 90^\circ$) and three outputs ($K = 3$) are produced using the directions $(\hat{\theta}_0, \phi_k)$. In the PTR segment, \hat{H} is the estimated channel impulse response and $*$ stands for conjugate. N feed-forwards and a single feedback filter are w_n^{ff} and w^{fb} , respectively, δ_n are phase-carries from PLL, and \hat{d} and \tilde{d} are soft and hard decision symbols, respectively.

decision feedback equalizer (DFE). This structure differs from standard communication structures in the following aspects: noise normalization, which has demonstrated an advantage for balancing vector sensor channels when using experimental data; beam steering, where directions are properly chosen to improve the coherence of vertical and horizontal component combinations; and the passive time-reversal, which has horizontal components weighted according to the joint direction information, attenuating possible noisy components, and the channels combining is performed after the first stage of the equalizer, enhancing coherence combination.

The first step shown in Fig. 2 is noise normalization, which aims to reduce noisy channels' degradation. One possible normalization approach uses the output noise variance, calculated using a training sequence, the estimated CIR, and the received signals [15]. However, since CIR estimation may depend on the configuration setup (replica, windowing, threshold), it may not be efficient for noisy channels. Here, we adopt a noise normalization where the objective is to balance vector sensor components according to the input noise variance. The noise variance is calculated in the signal bandwidth during the interval without transmission. The weight (η) for the n -th component is given by:

$$\eta_n = \frac{\frac{1}{\sigma_n^2}}{\sum_{i=1}^N \frac{1}{\sigma_i^2}}, \quad (6)$$

where σ_i^2 is the noise power of the i -th component of a single vector sensor with N components. The result of (6) can be equivalently obtained by the maximum likelihood estimation (MLE) and the effect is felt in the radiation pattern, which tends to result in a cardioid-like pattern. The interested reader may find a full study on the benefits of this noise normalization in [18], which is not the subject of analysis in this work.

The second step is the Doppler compensation. The adopted approach is based on the ambiguity function method using a block Doppler estimation [19]. A bank of correlators, represented as C in Fig. 2, is used to estimate the CIR. Interleaved m-sequence packets are used as replicas in this estimation. Then, time compression/expansion (Δ) is estimated between two subsequent packets. In practice, the use of one horizontal particle velocity component to estimate Δ is preferable to all components. This avoids possible fluctuation in the Δ estimation caused by late arrivals [18]. The output of the Doppler compensation stage are resampled signals according to the Δ factor, where z_p, z_{vx}, z_{vy} , and z_{vz} are the Doppler compensated signals for the pressure and particle velocity components, respectively.

The third step is composed of beam steering and passive time-reversal. The former is based on beamforming, where combining correlated signals and uncorrelated noise enhances SNR. Thus, the objective is to form a steerable beam, which results in directional gain [2]. Combining weighted vector sensor components, the k -th output ($k = 1 : K$, where $K = 3$) is given by:

$$y_k = z_p + z_{vx}u_{kx} + z_{vy}u_{ky} + z_{vz}u_{kz}, \quad (7)$$

where, $u_{kx} = \cos(\phi_k)\cos(\hat{\theta}_0)$, $u_{ky} = \cos(\phi_k)\sin(\hat{\theta}_0)$, and $u_{kz} = \sin(\phi_k)$ are scalar values calculated according to chosen angles. Here, DoA estimation is used to provide only the azimuth angle $\hat{\theta}_0$, whereas three elevation angles are fixed ($\phi_k = -90^\circ, 0^\circ, 90^\circ$). Note that using these elevation angles is equivalent to steer to surface ($\phi_1 = -90^\circ$), azimuth ($\phi_2 = 0^\circ$), and bottom ($\phi_3 = 90^\circ$). The option to use DoA to estimate the elevation was discarded for two reasons: first, steering to source direction, in terms of elevation, does not necessarily result in a minimum error for communications [20]; second, it was already shown that conventional DoA estimation methods, such as intensity-based, Bartlett,

minimum variance distortionless response (MVDR), in a multipath environment, may not provide accurate elevation angles [2].

The advantage of those three beam steering outputs is that we are providing combinations, as input for the equalizer, assuming a high correlation between pressure and vertical components, or pressure and the horizontal component in the estimated azimuth direction. For the azimuth, the DoA provides an accurate estimation angle, which benefits SNR. Here, the Bartlett estimator is used, where the azimuth angle is the maximum of the beam pattern response given by:

$$\hat{\theta}_0 = \arg \max_{\theta} \left\{ \mathbf{a}(\theta)^H \hat{R} \mathbf{a}(\theta) \right\}, \quad (8)$$

where $\mathbf{a} = [1 \ \mathbf{u}]^T$ with $\mathbf{u} = [\cos(\theta) \ \sin(\theta)]$ is the vector sensor array manifold, \hat{R} is the data estimated correlation matrix, and H is the Hermitian operator. A receiver structure composed only of the beam steering segment, named vs-bs, is tested in Sec. V.

The other segment of the joint method is the passive time-reversal. PTR is a method widely investigated in UWAC when arrays of pressure sensors are employed [21]–[24]. The method is computationally simple, although the performance can be severely degraded if CIR estimation is not accurate, which is still a challenging subject [22], [25]. PTR has been used in vector sensor receivers as an attempt to explore diversity [15], which came from the inherent directionality of vector sensor components (or orthogonality) shown in the correlation analysis (see Sec. III). However, using components of a 3D vector sensor indiscriminately in the PTR may not be a proper approach. For instance, if a sound wave arrives in the direction of one horizontal axis, this sound wave is substantially attenuated in the orthogonal axis direction. Thus, one horizontal component would simply add noise to the PTR without any benefit. Here, we employ a soft normalization, using the azimuth weights estimated for the beam steering. This approach attenuates possible noisy horizontal components. The m -th adapted PTR output ($m = 1 : M$, where $M = 4$) is given as:

$$p_m(t) = \hat{h}_m^*(-t) z_m(t) \mathbf{u}_m, \quad (9)$$

where $\mathbf{u}_m = 1$, for $m = 1$ and $m = 4$ (pressure and vertical particle velocity components), $\mathbf{u}_m = \mathbf{u}_x = \cos(\hat{\theta}_0)$ for $m = 2$, and $\mathbf{u}_m = \mathbf{u}_y = \sin(\hat{\theta}_0)$ for $m = 3$. z_m represents the Doppler compensated signals, where m from 1 to 4 are the pressure and particle velocity components (i.e., z_p , z_{vx} , z_{vy} , and z_{vz}), respectively. Note that (9) does not add any extra computational requirement compared to the standard PTR. In this study, the standard method is also used for comparison purposes, where the input are either vector sensor components, called vs-ptr, or pressure-only components, named p-ptr.

The last step in Fig. 2 is a multichannel DFE used for ISI mitigation. A second-order phase-locked loop (PLL) is embedded in the DFE for carrier-phase tracking (δ). Moreover, adaptive recursive least-square (RLS) algorithm is used to update the coefficient of N feed-forwards (w^{ff}) and one

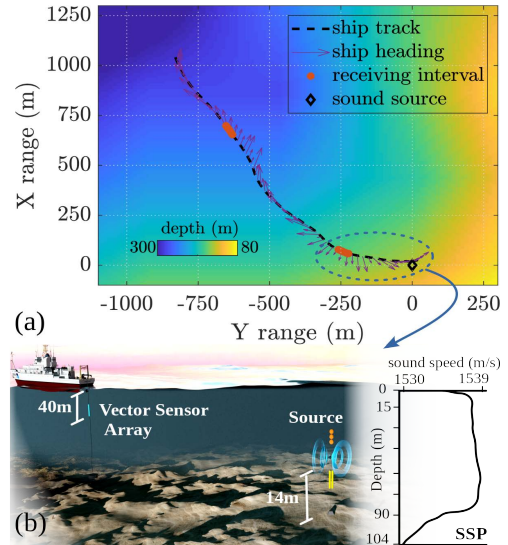


FIGURE 3. MakaiEx scenario: ship trajectory over X-Y area bathymetry centered at sound source position (22.1660 N; -159.7870 W), and receiving intervals (red dots) (a); vector sensor array tied at the ships' stern, sound source at approximately 90 m depth, and the sound speed profile (b).

feedback (w^{fb}) filters [26]. The multichannel DFE is also used for combining multiple vector sensors. Thus, the number of feed-forwards in total, N , is seven times the number of vector sensors.

V. RESULTS AND DISCUSSION

In this section, performance comparisons are made using simulation and experimental data. The simulated acoustic scenario is based on the Makai experiment (MakaiEx) [15], [18], [27]. In this experiment, a four-element vector sensor array (VSA) was tied at the research vessel Kilo Moana's stern, which was set in drift mode in a shallow-water area, off the coast of Kauai Island, Hawaii, in 2005 (see Fig. 3 (a)). The VSA was vertically kept at approximately 40 m depth, and communication signals were transmitted by a bottom-moored sound source placed at 90 m depth, where the local depth is 104 m (Fig. 3 (b)). Source-receiver ranges vary from approximately 20 m to 1.5 km, and two receiving intervals, at 230 and 907 m range, are used for experimental validation in this work. The vector sensor employed in the experiment is the accelerometer-based TV-001 model (Wilcoxon Research Inc) [15], [28]. Each vector sensor comprises three uni-axial accelerometers, orthogonally-oriented, and one hydrophone, approximately at the geometric center. These are encapsulated in neutrally buoyant resin, forming a 3.81×6.35 cm cylinder-type, and the spacing between vector sensors is approximately 10 cm.

In MakaiEx, the transmitted signal for coherent modulation is a binary phase-shift keying (BPSK), in the carrier frequency of 10 kHz and bandwidth of 2 kHz, filtered by a root-raised-cosine pulse shape with a roll-off factor of 0.5.

A. SIMULATION

The following simulation aims to understand and to test the receiver structures, especially those that depend on CIR

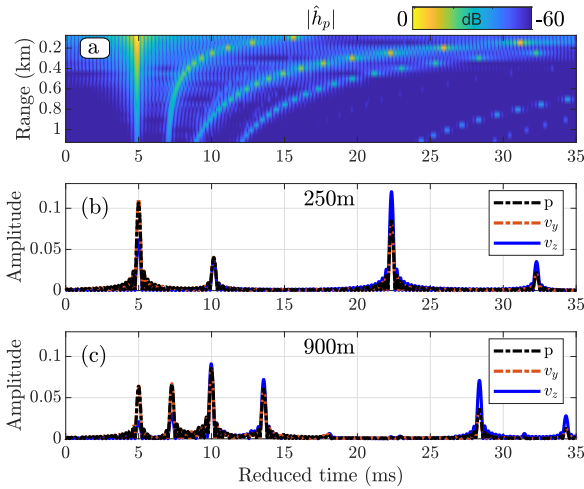


FIGURE 4. Channel impulse response for pressure versus range (a), and for pressure and particle velocity components (y, z) for 250 m (b) and 900 m (c).

estimation, where estimation errors in experimental data may affect the performance. The acoustic scenario is simulated using the OASES numerical model, where pressure, horizontal, and vertical particle velocity CIR are estimated for discrete ranges from 100 to 1100 m [29]. The simulation is performed using the sound speed profile (SSP) measured during MakaiEx (Fig. 3 (b)) and the bottom properties estimated in [4].

The estimated CIR for pressure along range is shown in Fig. 4 (a). The first arrival (5 ms) is the direct path, followed by the bottom-bounce, surface-bounce, and bottom-surface reflection. One can notice that late arrivals, from surface and bottom reflections, become closer to the first as the range increases, which is an expected result for the source-receiver geometry. Fig. 4 (b) and (c) shows the pressure (p), horizontal (v_y), and vertical (v_z) particle velocity CIR, normalized to unitary power, for 250 and 900 m, respectively. In Fig. 4 (b), pressure and horizontal particle velocity channels present similar amplitudes. Moreover, the first arrival amplitude is larger than late arrivals (i.e., minimum phase [30]). On the other side, the vertical component has the highest amplitude for the third arrival, which is expected since the surface arrival has a steeper AoA. In Fig. 4 (c), the third arrival has a higher amplitude than the first one for all components, which can be assigned to the sound refraction due to a non-isovelocity SSP, and that we seek for confirmation with the real data.

Table 1 shows the RMS delay-spread (DS) and the cross-correlation among vector sensor channels (see [31] for correlation and [32] for DS calculations). Results of Table 1 were obtained using a 35 ms window, as presented in Fig. 4. The horizontal particle velocity DS (DS-y) presents lower or equal values than the DS of pressure (DS-p) for all calculated ranges. Considering DS as a channel severity measure, using the horizontal particle velocity component may be advantageous to the pressure component. Values of vertical particle velocity DS (DS-z) are lower than DS-p/DS-y for ranges

TABLE 1. RMS delay spread (DS-*) and vector sensor channel correlation (C*) for several source-receiver ranges. Delay spread and correlation are calculated for/between pressure (p), horizontal (y) and vertical (z) particle velocity components.

Range (m)	100	250	400	550	700	850	1000
DS-p (ms)	14.25	9.72	7.71	6.87	8.78	8.84	9.05
DS-y (ms)	13.21	9.63	7.71	6.83	8.67	8.76	8.99
DS-z (ms)	15.10	9.36	7.23	6.68	10.22	10.06	9.51
C ^{py}	0.99	1.00	1.00	1.00	1.00	1.00	1.00
C ^{pz}	0.57	0.61	0.52	0.46	0.35	0.31	0.33
C ^{yz}	0.61	0.64	0.53	0.46	0.36	0.31	0.34

from 250 to 550 m, but higher than those at other ranges. This can be related to steeper AoA at shorter ranges (<250 m), and late arrivals at longer ranges (>550 m).

Correlation between pressure and the horizontal particle velocity channel (C^{py}) shows values over 0.99, indicating high similarity, as predicted in Section III. Table 1 also shows the correlation between pressure and the vertical particle velocity channels (C^{pz}), and the particle velocity cross-correlation (C^{yz}). One can note that C^{pz} ≈ C^{yz} ≈ 0.6 for short ranges (<250 m). For other ranges, correlation becomes lower (<0.5), which is also an expected result, according to the analysis of Section III.

Fig. 5 shows communication performance using bit error rate (BER) analysis: along range for fixed SNR = 4 dB (a) and versus SNR at ranges of 250 m (b) and 900 m (c). The tested receivers are: PTR using a single pressure component (p-ptr); standard PTR using the three vector sensor components (vs-ptr); beam steering (vs-bs); and the joint method (vs-bsptr). In this simulation, the transmitted signal with the MakaiEx setup was used, containing two packets of 1 s each, filtered by the CIR provided by OASES numerical model. Noise normalization, Doppler compensation, and the PLL were not used in the simulation. Furthermore, when PTR is used, CIR estimation is performed using a window duration of 35 ms.

In Fig. 5 (a), the performance of p-ptr varies around 8%, whereas using a single vector sensor with PTR (vs-ptr), the error is lower than 1.5% along range. The vs-ptr performance is better than vs-bs in general, except for short ranges (<150 m), where the correlation between pressure and

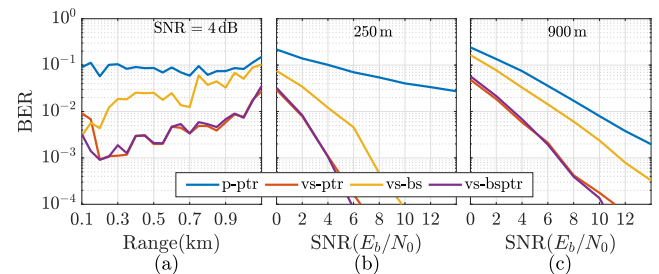


FIGURE 5. One pressure sensor and a single vector sensor comparison. BER versus range (a), and BER versus SNR for 250 m (b) and 900 m (c). p-ptr represents a single pressure sensor followed by PTR and equalizer; vs-ptr is the standard PTR using vector sensor channels; vs-bs is the beam steering method; vs-bsptr is the proposed joint method.

vertical particle velocity channels is high. One can notice that such results were obtained using the CIR from OASES numerical acoustic model, and thus, it was expected that some variation could be present in the performance along range. This result suggests that the vs-bs may be more appropriate for short ranges than the vs-ptr. The vs-bsptr maintains the vs-ptr advantage when diversity can be explored at longer ranges and beamforming for shorter ranges, presenting errors lower than 1.5%, even for low SNR (4 dB). The BER versus SNR analysis of Fig. 5 (b) and (c) shows that using vs-bsptr, errors are lower than 10^{-4} for SNR > 6 dB at 250 m, and SNR > 10 dB at 900 m.

Although vs-bs shows higher errors than both vs-ptr and vs-bsptr, we should be aware that imprecision in the channel estimation can degrade performance of PTR in experimental data. Moreover, one can notice that azimuth estimation was not taken into account for the simulation, which is a vs-bs benefit. Thus, based on the simulation results, for the experimental data, we expect: an advantage of vs-bs in shorter ranges, raised by the azimuth gain; a penalty in the PTR performance due to channel estimation imprecision; and a robust performance for vs-bsptr, taking advantage of both approaches. Thus, those simulation results serve, at least, as an initial insight of the performance, which agrees with the theoretical assumption that beamforming is more advantageous at shorter ranges and diversity for longer ranges.

B. EXPERIMENTAL DATA ANALYSIS

For experimental data, we analyze 90 packets transmitted at 230 and 907 m source-receiver ranges. Each packet lasts 1 s and has 2k symbols, in which the first 255 symbol m-sequence is used for Doppler compensation and channel estimation. The forget factor $\lambda = 0.998$, proportional and integral factors, $k_p = 0.01$ and $k_I = 0.001$, were set in RLS and PLL, respectively. These values are used for both ranges to check robustness empirically. The number of feed-forward and feedback filters, for a fractionally spaced equalizer, are 30 and 10, respectively. One can notice that the CIR and BER analyses are used to quantify performance for experimental data. Although analysis of the SNR after vs-bs and vs-ptr stages could be used, a clear relation between such SNR improvement and performance was not found, and thus, SNR is not analyzed here.

Fig. 6 shows the estimated channel impulse response for the y-axis of vector sensor #1, the closest to the surface, for source-receiver ranges of 230 m (a) and 907 m (b). Although first arrival amplitudes do not present fading, temporal coherence of vector sensor channels varies from 500 ms to 700 ms. Fig. 7 shows pressure and particle velocity CIR for the respective transmitted ranges, estimated taking the 90 s time average. One can notice the ray arrival time coincidence to those predicted in simulation (see Fig. 4). However, the exact match in amplitude is hard to be guaranteed considering several surface and bottom effects present in real data, as noticed for the third arrival (surface reflection) of $|\hat{h}_{vz}|$ in Fig. 7 (a) and Fig. 4 (b). In this range, the multiple AoAs tend to be

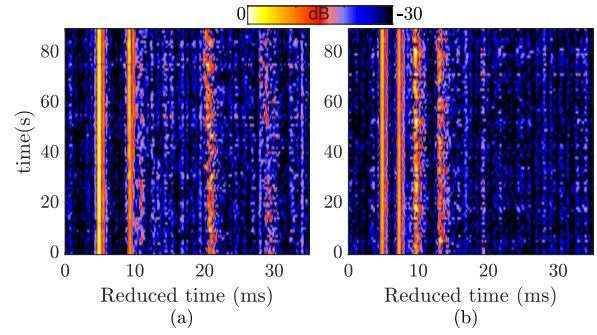


FIGURE 6. Estimated time-varying channel impulse response for y-axis of vector sensor #1 (the closest to the surface) using 255 symbols preamble, for source-receiver range of 230 m (a) and 907 m (b).

steeper than that found at 907 m, and the surface effects, such as scattering and roughness, may have a substantial impact, not considered in the simulation. For 907 m, the vertical component's amplitude ($|\hat{h}_{vz}|$) shows the third arrival with larger amplitude than the first one, as predicted in simulation. Since the vector sensor vertical component filters horizontal arrivals, the direct path is more attenuated than the surface reflection (third arrival) at 907 m. Thus, this explains the first two arrivals attenuated in Fig. 7 (b) for the vertical component. Moreover, comparing the CIR among vector sensor components in Fig. 7 (a) and Fig. 7 (b), the latter shows a more diverse channel.

Fig. 8 shows the BER performance for each vector sensor individually (vs_n) and for the four-element pressure-only array (p-only). A pair of numbers is printed next to each error. These two numbers represent, for a total of 90 packets, the number of packets with zero BER (i.e., it was not possible to measure errors for the considered number of samples) and the number of packets with BER > 10%.

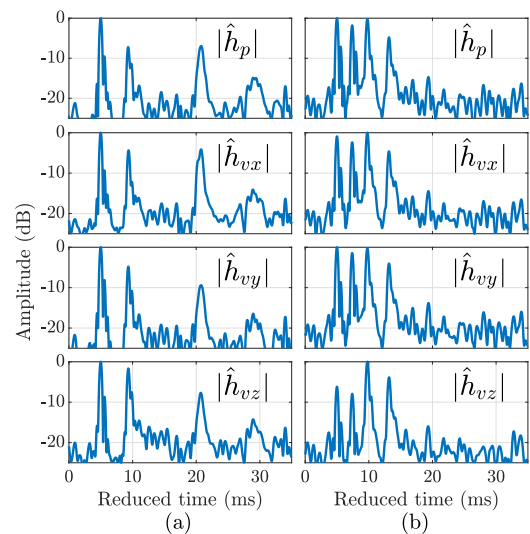


FIGURE 7. Estimated channel impulse response for pressure (p) and particle velocity channels (x,y,z) from top to bottom, for source-receiver ranges of 230 m (a) and 907 m (b).

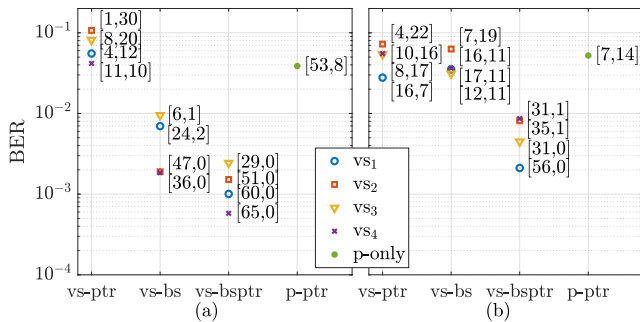


FIGURE 8. BER performance for the tested receivers for each vector sensor, for source-receiver range of 230 m (a) and 907 m (b). For reference, the pressure-only array performance (p-only, using 4 hydrophones) is shown using a standard PTR (p-ptr). The numbers next to each error represent [number of packets BER=0, number of packets BER>10%].

Fig. 8 (a) shows the performance for 230 m range. Using the vs-ptr, performance varies from 4% to 10%, which is the worst performance among the tested receivers. However, the vs-ptr performance of vector sensor #4 is comparable to p-ptr, which means, at least, a size reduction improvement. vs-bs presents BER from 0.2% to 1%, whereas vs-bsptr varies from 0.06% to 0.3%. For this source-receiver range, the beam steering segment is advantageous in the vs-bsptr, resulting in the lowest error, on average, among vector sensors. In Fig. 8 (b), BER for 907 m range is shown, where similar performance is noticed between vs-ptr, vs-bs, and p-ptr, on average. vs-bsptr shows BER from 0.2% to 0.8% among vector sensors, which is about ten times less error than individual approaches. The obtained results for the tested ranges reinforce the hypothesis, predicted in simulation, that: the beamforming approach is beneficial at the shorter range; the PTR approach is degraded due to channel estimation variability; and vs-bsptr can take advantage of both methods. An important aspect is that the performance varies up to eight times among vector sensors for the same structure. Thus, the performance analysis of only one vector sensor could lead to a premature conclusion, which motivated the quantification of individual vector sensors to a secure interpretation.

Fig. 9 shows the BER performance combining the vector sensors. In this figure, performance is shown for a single

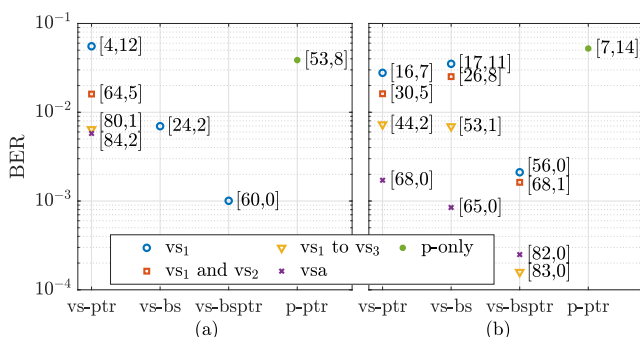


FIGURE 9. BER performance for the tested receivers combining vector sensors, for source-receiver range of 230 m (a) and 907 m (b). For reference, the pressure-only array performance (p-only, using 4 hydrophones) is shown using a standard PTR (p-ptr). The numbers next to each error represent [number of packets BER=0, number of packets BER>10%].

vector sensor (enumerated as vector sensor #1), combining multiple vector sensors (up to four in the VSA), and the pressure-only array, for the two mentioned source-receiver ranges. In Fig. 9 (a), except for vs-ptr, combining two vector sensors (vector sensor #1 and vector sensor #2) or more, result in errors below 10^{-4} (not shown in the figure). These obtained results also reinforce that the beamforming approach is beneficial at this range. vs-ptr performance is improved as the number of sensors increases, which is an expected result as spatial diversity may be found among sensors of the array. In Fig. 9 (b), vs-ptr shows similar performance to vs-bs, which indicates that diversity is better explored in this range. Combining the methods in vs-bsptr produces the best performance, which varies from 0.2%, for vector sensor #1 to 0.016% for the VSA.

VI. CONCLUSION

This paper shows the performance of acoustic vector sensor receiver structures used for underwater communications. Vector sensor channels are explored, taking advantage of diversity and beamforming. The joint vector sensor beam steering and passive time-reversal receiver structure is proposed with the idea of exploring high/low correlated vector sensor components.

In a first phase, simulation has served as an initial insight of the various receivers' performance. Results have indicated the advantage of the beam steering at shorter ranges and the PTR at longer ranges, which was also verified with field data acquired during the MakaiEx. For real data, the joint method has reduced the error by around ten times compared to separate approaches, using a single vector sensor for the longer analyzed range. It is also shown the usual comparison between a single vector sensor or a VSA and an aperture pressure-only array, where a single vector sensor may outperform the pressure-only array. However, here, it is shown that the joint method can achieve further performance enhancement. Although longer ranges (> 1000 m) need to be explored using experimental data, these promising results motivate the optimization of communication structures properly designed for vector sensors instead of the standard ones.

In summary, the contributions of this work are: propose a joint method structure designed for vector sensors and compare it to standard structures; reinforce the proper use of the directional information, where theoretical analysis of correlation among pressure and particle velocity channels helps to understand the particularities of each tested structure; shows a wide comparison, using vector sensors individually and combining multiple vector sensors, where the reader can verify and get an insight of a trade-off between array size and the communication performance.

At last, the receiver structures tested in this work are expected to work as practical tools for real-time applications used in size-restricted platforms. We have seen that superior performance is achieved by combining vector sensors in a VSA. However, it comes with computational expenses as the number of channels increases in the multichannel equalizer.

Thus, future investigations can be performed by optimizing the channel selection instead of using all VSA channels.

ACKNOWLEDGMENT

The authors would like to thank Makai's research group: M. Porter (chief scientist), J. Tarasek (vector sensor array), P. Hursky, M. Siderius, and B. Abraham (data acquisition assistance), and the help of the UALg team: A. Silva and F. Zabel. The Makai Experiment was supported by ONR.

REFERENCES

- [1] A. Nehorai and E. Paldi, "Acoustic vector-sensor array processing," *IEEE Trans. Signal Process.*, vol. 42, no. 9, pp. 2481–2491, Sep. 1994.
- [2] P. Felisberto, O. Rodriguez, P. Santos, E. Ey, and S. M. Jesus, "Experimental results of underwater cooperative source localization using a single acoustic vector sensor," *Sensors*, vol. 13, no. 7, pp. 8856–8878, 2013.
- [3] S. M. Jesus, F. C. Xavier, R. P. Vio, J. Osofsky, M. V. S. Simões, and E. B. F. Netto, "Particle motion measurements near a rocky shore off cabo frio island," *J. Acoust. Soc. Amer.*, vol. 147, no. 6, pp. 4009–4019, Jun. 2020.
- [4] P. Santos, O. C. Rodríguez, P. Felisberto, and S. M. Jesus, "Seabed geoaoustic characterization with a vector sensor array," *J. Acoust. Soc. Amer.*, vol. 128, no. 5, pp. 2652–2663, Nov. 2010.
- [5] A. Abdi, H. Guo, and P. Suthiwan, "A new vector sensor receiver for underwater acoustic communication," in *Proc. OCEANS*, Sep. 2007, pp. 1–10.
- [6] C. H. Sherman and J. L. Butler, *Transducers Arrays for Underwater Sound*. New York, NY, USA: Springer New York, 2007.
- [7] T. Gabrielson, "Design problems and limitations in vector sensors," in *Proc. Workshop Directional Acoustic Sensors (NUWCD ONR)*, Newport, Rhode Island, Apr. 2001, pp. 29–48.
- [8] K. Kim, T. B. Gabrielson, and G. C. Lauchle, "Development of an accelerometer-based underwater acoustic intensity sensor," *J. Acoust. Soc. Amer.*, vol. 116, no. 6, pp. 3384–3392, Dec. 2004.
- [9] T. B. Gabrielson, D. L. Gardner, and S. L. Garrett, "A simple neutrally buoyant sensor for direct measurement of particle velocity and intensity in water," *J. Acoust. Soc. Amer.*, vol. 97, no. 4, pp. 2227–2237, 1995.
- [10] X.-Y. Xu, H. Ge, J. Zhao, Z.-F. Chen, J. Zhang, M.-H. Lu, M. Bao, Y.-F. Chen, and X.-D. Li, "A monolithic three-dimensional thermal convective acoustic vector sensor with acoustic-transparent heat sink," *JASA Exp. Lett.*, vol. 2, no. 4, Apr. 2022, Art. no. 044001.
- [11] T. C. Yang, "A study of spatial processing gain in underwater acoustic communications," *IEEE J. Ocean. Eng.*, vol. 32, no. 3, pp. 689–709, Jul. 2007.
- [12] S. Chandran, *Adaptive Antenna Arrays: Trends and Applications*, 1st ed. Berlin, Germany: Springer, 2004.
- [13] A. Abdi and H. Guo, "Signal correlation modeling in acoustic vector sensor arrays," *IEEE Trans. Signal Process.*, vol. 57, no. 3, pp. 892–903, Mar. 2009.
- [14] M. Hawkes and A. Nehorai, "Acoustic vector-sensor correlations in ambient noise," *IEEE J. Ocean. Eng.*, vol. 26, no. 3, pp. 337–347, Jul. 2001.
- [15] A. Song, A. Abdi, M. Badiéy, and P. Hursky, "Experimental demonstration of underwater acoustic communication by vector sensors," *IEEE J. Ocean. Eng.*, vol. 36, no. 3, pp. 454–461, Jul. 2011.
- [16] L.-X. Guo, X. Han, J.-W. Yin, and X.-S. Yu, "Underwater acoustic communication by a single-vector sensor: Performance comparison using three different algorithms," *Shock Vibrat.*, vol. 2018, pp. 1–8, Nov. 2018.
- [17] X. Han, J. Yin, Y. Tian, and X. Sheng, "Underwater acoustic communication to an unmanned underwater vehicle with a compact vector sensor array," *Ocean Eng.*, vol. 184, pp. 85–90, Jul. 2019.
- [18] F. D. A. Bozzi and S. M. M. Jesus, "Acoustic vector sensor underwater communications in the Makai experiment," in *Proc. Meetings Acoust.*, Jul. 2021, Art. no. 070029.
- [19] B. S. Sharif, J. Neasham, O. R. Hinton, and A. E. Adams, "A computationally efficient Doppler compensation system for underwater acoustic communications," *IEEE J. Ocean. Eng.*, vol. 25, no. 1, pp. 52–61, Jan. 2000.
- [20] F. D. A. Bozzi and S. M. Jesus, "Vector sensor beam steering for underwater acoustic communications," in *Proc. Meetings Acoust.*, 2020, Art. no. 070002.

- [21] J. A. Flynn, J. A. Ritcey, D. Rouseff, and W. L. J. Fox, "Multichannel equalization by decision-directed passive phase conjugation: Experimental results," *IEEE J. Ocean. Eng.*, vol. 29, no. 3, pp. 824–836, Jul. 2004.
- [22] T. C. Yang, "Differences between passive-phase conjugation and decision-feedback equalizer for underwater acoustic communications," *IEEE J. Ocean. Eng.*, vol. 29, no. 2, pp. 472–487, Apr. 2004.
- [23] J. Gomes, A. Silva, and S. Jesus, "Joint passive time reversal and multi-channel equalization for underwater communications," in *Proc. OCEANS*, Sep. 2006, pp. 1–6.
- [24] J. Gomes, A. Silva, and S. Jesus, "Adaptive spatial combining for passive time-reversed communications," *J. Acoust. Soc. Amer.*, vol. 124, pp. 1038–1053, Aug. 2008.
- [25] J. Zheng, T. Yang, H. Liu, and T. Su, "Efficient data transmission strategy for IloTs with arbitrary geometrical array," *IEEE Trans. Ind. Informat.*, vol. 17, no. 5, pp. 3460–3468, May 2021.
- [26] J. G. Proakis and M. Salehi, *Digital Communications*, 5th ed. Boston, MA, USA: McGraw-Hill, 2008.
- [27] M. Porter, B. Abraham, M. Badiéy, M. Buckingham, T. Folegot, P. Hursky, S. Jesus, B. Kraft, V. McDonald, and W. Yang, "The Makai experiment: High-frequency acoustics," in *Proc. 8th Eur. Conf. Underwater Acoust., Carvoeiro, Portugal*, 2012, p. 10.
- [28] J. C. Shippis and B. M. Abraham, "The use of vector sensors for underwater port and waterway security," in *Proc. ISA/IEEE Sensors Ind. Conf.*, Jan. 2004, pp. 41–44.
- [29] H. Schmidt, "Oases—User guide and reference manual," Dept. Ocean Eng., Massachusetts Inst. Technol., Cambridge, MA, USA, Tech. Rep., Oct. 2004, vol. 3.1.
- [30] T. C. Yang, "Correlation-based decision-feedback equalizer for underwater acoustic communications," *IEEE J. Ocean. Eng.*, vol. 30, no. 4, pp. 865–880, Oct. 2005.
- [31] T. C. Yang, "Measurements of temporal coherence of sound transmissions through shallow water," *J. Acoust. Soc. Amer.*, vol. 120, no. 5, pp. 2595–2614, Nov. 2006.
- [32] T. S. Rappaport, *Wireless Communications: Principles and Practice*, 2nd ed. Upper Saddle River, NJ, USA: Prentice-Hall, 2002, p. 199.



FABRICIO A. BOZZI received the B.S. and M.S. degrees in electrical engineering from the Federal University of Rio de Janeiro, Brazil, in 2012 and 2016, respectively. He is currently pursuing the Ph.D. degree in electronics and telecommunications engineering with the University of Algarve, Portugal.

From 2013 to 2019, he was involved in the development of signal processing tools for passive and active sonar systems at the Brazilian Navy Research Institute. His research interests include array signal processing, sonar systems, acoustic vector sensors, and underwater communications.



SÉRGIO M. JESUS (Member, IEEE) received the Doctorat Es-Sciences degree in engineering sciences from the Université de Nice, Nice, France, in 1986.

From 1986 to 1992, he was a Staff Scientist with the SACLANT Undersea Research Centre, La Spezia, Italy, in the ambient noise and Signal Processing Groups. During that period he was involved with underwater acoustic field noise directionality and early studies on target detection using matched field processing. In 1992, he joined the Department of the Electrical Engineering and Computer Science, University of Algarve, Faro, Portugal, where he is currently a Full Professor. He has coordinated EU projects UAN and OAEx. His research interests include underwater acoustics array signal processing, model-based inversion, ocean and seafloor tomography, and underwater acoustic communications.

Dr. Jesus is a member of the IEEE Signal Processing Society and of the Acoustical Society of America.